 doi:10.20944/preprints201611.0088.v1

Article

Tuneable Photonic Fiber Bragg Grating for Magnetic Field Sensor

Farah S. Al-Thahapy, Anwaar A. Al-Dergazly *

Department of Laser and optoelectronics Engineering, Al-Nahrain University, Baghdad, Iraq; galaxy.tota92@yahoo.com

* Correspondence: aldergazly@eng.nahrainuniv.edu.iq or aldergazly@gmail.com; Tel.: +94-772-546-2643

Abstract: In this project, four of fibers Bragg gratings were fabricated by injecting different volumes of liquids (star line Glass Mechanix optical adhesive material, olive oil diluted with ethanol) into the hollow core fiber. The amplitude splitting interferometric technique with a high resolution specially designed translation stage was used for the fabrication process. The fabrication was done using ultraviolet laser operated at wavelength 405nm. The fabricated Bragg length of the four fibers is equal to 3.8 cm. The results presented fiber Bragg grating (FBG) with successful fabrication at 653.3 nm Bragg reflected wavelength.

Keywords: fiber Bragg grating; photonic crystal fiber; photosensitivity; FBG magnetic field sensor; olive oil; optical adhesive

1. Introduction

The discovery of optical fibers has developed the field of telecommunications. Over the past three decades, the developments in optical fiber has certainly improved and reshaped fiber optic technology. In addition to applications in telecommunications, optical fibers are also used in the fields of fiber optics sensors, fiber optics lasers, and fiber optics amplifiers. Despite the enhancements in optical fiber manufacturing and progressions in the field in general, basic optical components have been a challenge to integrate with fiber optics, such as mirrors, wavelength filters, and partial reflectors. In recent times, all these have been improved with the ability to change the core refractive index in an optical fiber using optical absorption of ultraviolet (UV) light. This photosensitivity of optical fibers allows the fabrication of grating planes in the core of fibers. These gratings planes are obtained by permanently varying the refractive index in a periodic form along the core of the fiber. A periodic variation of the refractive index in the fiber core acts like a wavelength selective mirror that satisfies the Bragg condition i.e. it forms a fiber Bragg grating. The grating period and length of the grating, together with the strength of the variation of the refractive index, limited whether the grating had a high or low reflection over a wide or narrow range of wavelengths [1].

2. Fiber Bragg Gratings Principles

Gratings in a fiber are fabrication result of periodic perturbations within the fiber core. The perturbations known as grating planes are generally formed by exposing the fiber core to a UV light interference pattern, which increases the core refractive index (n_{Core}) at the points of exposure. In

Preprints (www.preprints.org) | NOT PEER-REVIEWED | Posted: 17 November 2016 doi:10.20944/preprints201611.0088.v1

the simplest form, the grating planes are perpendicular to the fiber length and have a constant grating period as the assumption is made and it's shown in Figure 1 [2].

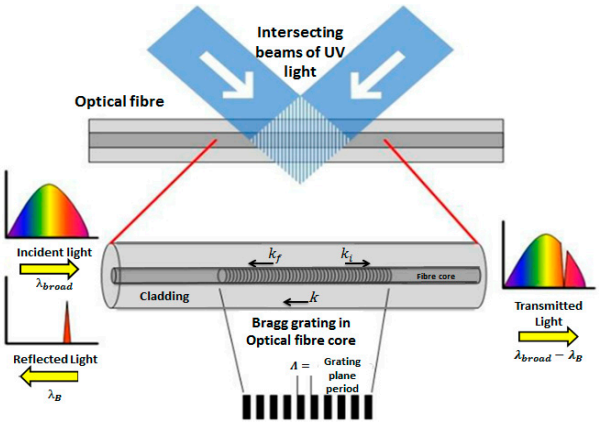

Figure 1. Illustration of uniform Bragg grating inside a fiber [2].

Phase match between the incident light that is directed along the fiber and the grating planes is required in order to reflect the light back within the core of the waveguide along counter propagating modes to meet the Bragg condition and it's defined by equation (1) [2]:

$$2 \times \Lambda \times \sin\Theta = n \times \lambda \quad \ldots (1)$$

where Λ is the grating planes period, θ is the angle between the scattering planes and the incident light , n is an integer and λ is the incident light wavelength .

The reflected Bragg response has a center wavelength known as the Bragg reflected wavelength (λ_B) that is identified by the Bragg grating parameters. The grating planes are shown in the illustration of Figure 1 as steps of index variation; however a factual illustration would look like nearer to a sinusoidal variation of refractive index along the waveguide core. The Bragg condition is met if energy and momentum is preserved. Energy preservation ($\Box\omega_f = \Box\omega_i$) needs that the reflected radiation frequency to be equal to the incident frequency. Momentum preservation requests that the summation of the incident wave vector (k_i) and the grating wave vector (k) is equivalent to the scattered radiation wave vector (k_f) as given in equation (2) [2]:

$$k_i + k = k_f \quad \ldots (2)$$

When the grating wave vector (k) is perpendicular to the grating planes, then it will be equivalent to $2 \times \pi/\Lambda$. Incident wave vector and diffracted wave vector are the same in the magnitude but reverse in the direction, so the momentum preservation condition will be as follow [2]:

$$2 \times \left(\frac{2 \times \pi \times n_{eff}}{\lambda_B}\right) = \frac{2 \times \pi}{\Lambda} \quad \ldots (3)$$

Equation (3) is simplified to give Bragg condition for the first order as follow:

$$\lambda_B = 2 \times n_{eff} \times \Lambda \quad \ldots (4)$$

Where λ_B is the Bragg wavelength, which is the center wavelength of the reflected response and n_{eff} is the effective refractive index of the fiber core along Bragg grating length [2].

Equation (5) is used to obtain the number of grating planes N [3]:

Preprints (www.preprints.org) | NOT PEER-REVIEWED | Posted: 17 November 2016 doi:10.20944/preprints201611.0088.v1

$$N = \frac{l}{\Lambda} \quad \ldots (5)$$

where: l is Bragg grating length.

For a uniform FBG inscribed in the optical fiber core with an index of refraction n_{eff}. Then index of refraction profile n(x)is given as follow [4]:

$$n(x) = n_{eff} + \Delta n \cos\left(\frac{2 \times \pi \times x}{\Lambda}\right) \quad \ldots (6)$$

where Δn is the amplitude of the refractive index perturbation and x is the distance along the fiber longitudinal axis. The grating reflectivity with constant amplitude modulation and period can be described as follow [4]:

$$R(l,\lambda)_{MAX.} = \frac{\Omega^2 \times \sinh^2(s \times l)}{\Delta k^2 \times \sinh^2(s \times l) + s^2 \times \cosh^2(s \times l)} \quad \ldots (7)$$

where $R(l,\lambda)_{MAX.}$ is the reflectivity, which is a function of Bragg grating length l and wavelength λ, Ω is the coupling coefficient, $\Delta k = k - \pi/\lambda$ is the wave vector detuning, $k = 2 \times \pi \times n_{eff}/\lambda$ is the propagation constant, and $s = \sqrt{\Omega^2 - \Delta k^2}$. The coupling coefficient Ω for the sinusoidal variation of index perturbation along the fiber longitudinal axis has been found as follow:

$$\Omega = \frac{\pi \times \Delta n \times \eta(V)}{\lambda} \quad \ldots (8)$$

where η(V)is a function of the normalized frequency V of the optical fiber that represents the fraction of the fiber mode power contained in the fiber core, $\eta(V) \approx 1 - V^{-2}$. The normalized frequency V is given as follow [5]:

$$V = \frac{2 \times \pi \times r}{\lambda} \sqrt{n_{Core}^2 - n_{Clad}^2} = \frac{2 \times \pi \times r}{\lambda} \times NA \quad \ldots (9)$$

where λ is incident light wavelength, r is the core radius, n_{Core} is the refractive index of the fiber core, n_{clad} is the refractive index of the fiber clad, NA is the numerical aperture.

At the Bragg wavelength, there is no wave vector detuning i.e. Δk equals zero, so the reflectivity becomes [4]:

$$R(l,\lambda)_{MAX.} = \tanh^2(\Omega \times l) \quad \ldots (10)$$

The reflection increases by the variation of the refractive index. The reflection also increases by the increase in Bragg grating length [4].

3. Amplitude Splitting Interferometry Technique [6]

This technique was first used by Meltz et. al. who proved FBG fabrication results when the fiber exposed with UV interference pattern vertically on its axis. This fabrication was done as a result of splitting the UV inscription beam into two equal intensity UV beams, and these two UV beams recombined generating UV interference pattern. Then this interference pattern was focussed using a cylindrical lens into the fiber core , using a cylindrical lens effect on increasing the pattern intensity and this improves the fabrication. Figure 2 shows an example of typical amplitude splitting interferometer technique. In this figure UV laser beam is guided to a beam splitter, this will split the UV laser beam into two equal intensity laser beams. Both are reflect by the mirrors and

Preprints (www.preprints.org) | NOT PEER-REVIEWED | Posted: 17 November 2016 doi:10.20944/preprints201611.0088.v1

heading for the fiber core where the two UV beams are recombined. This leads to formation of UV interference pattern in the core of the fiber. At the high intensity of this pattern, the index of refraction of the core of the optical fiber is permanently varied, thus forming Bragg grating planes.

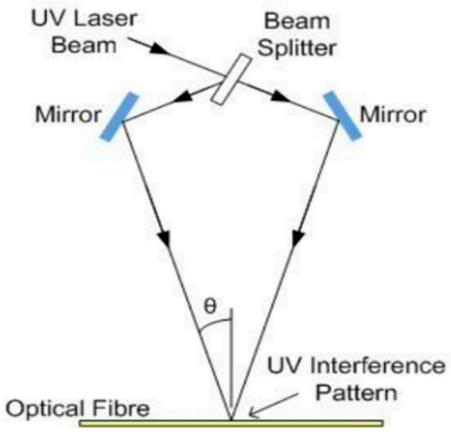

Figure 2. A typical arrangement of amplitude splitting interferometer technique [6].

The period (Λ) between the grating planes is known via the inscripting laser wavelength (λ_{UV}) and the separation angle (θ) between the two recombining UV laser beams and it's given as follow:

$$\Lambda = \frac{\lambda_{UV}}{2 \times \sin(\theta)} \quad \ldots (11)$$

Combining Equation (4) and Equation (11) the Bragg wavelength (λ_B) of the fabricated FBG can be known via the inscription laser wavelength (λ_{UV}) and the separation angle (θ) between the two recombining UV laser beams and it's given as follow:

$$\lambda_B = \frac{n_{eff} \times \lambda_{UV}}{\sin(\theta)} \quad \ldots (12)$$

where n_{eff} is the effective refractive index of the fiber core along the Bragg grating length.

4. Preparations of Bragg Materials

The key step used in this research is the chemical reaction of laser light effects on the photosensitive material (polymer adhesive material). The cure process of polymer adhesive depends on the intensity and the wavelength of the laser. This reaction causes optical variation in the properties of the adhesive material as well as in the index of refraction. It was mentioned before that FBG depends essentially on index of refraction variation. The material used in this process is star line Glass Mechanix adhesive, it is a colourless, clear liquid photo polymer adhesive and it has medium viscosity for bonding glass. This material is affected by the UV irradiation in a process termed "curing process", which is converting process from liquid state into solid material state. Ultraviolet-Visible (UV-VIS) spectrophotometer is used to obtain the absorption spectrum of star line Glass Mechanix adhesive material and it's shown in Figure 3.

Preprints (www.preprints.org) | NOT PEER-REVIEWED | Posted: 17 November 2016 doi:10.20944/preprints201611.0088.v1

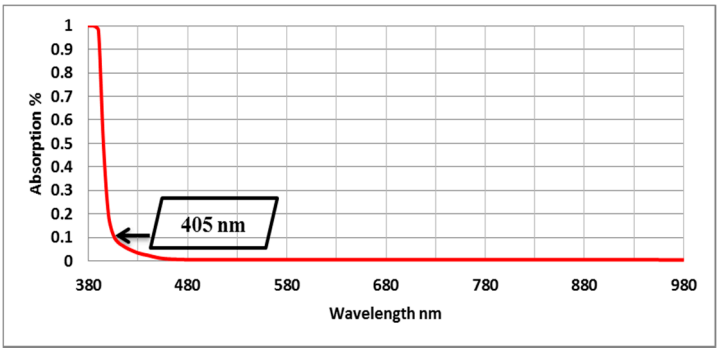

Figure 3. Illustrate the absorption of the polymer star line.

Figure 3 shows the adhesive material star line Glass Mechanix the maximum absorption. Actually, there is no such a laser available at that wavelength. So, the nearest and appropriate laser at wavelength 405 nm is used. Laser diode transmittance spectrum that used in the process of curing is given in Figure 4.

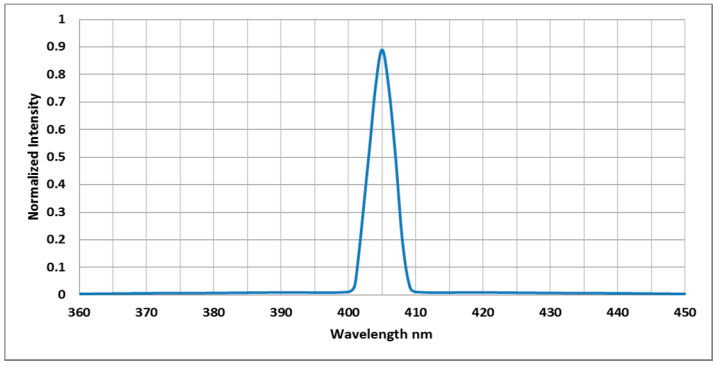

Figure 4. Laser diode spectrum of 405nm.

As given in Figure 3, the adhesive material has 10% absorption at a laser wavelength 405nm which makes it functional in this project but it needs extra time for cure. Additionally, the star line optical adhesive has a medium viscosity.

Olive Oil is an organic composite, it candidates to be used in photonics applications because it has a good nonlinear optical properties; It is used as a mixture with star line optical adhesive material. In this research, the type of olive oil is virgin. UV-VIS spectrophotometer is used for measuring the optical transmission of olive oil. Figure 5 shows olive oil transmission spectrum.

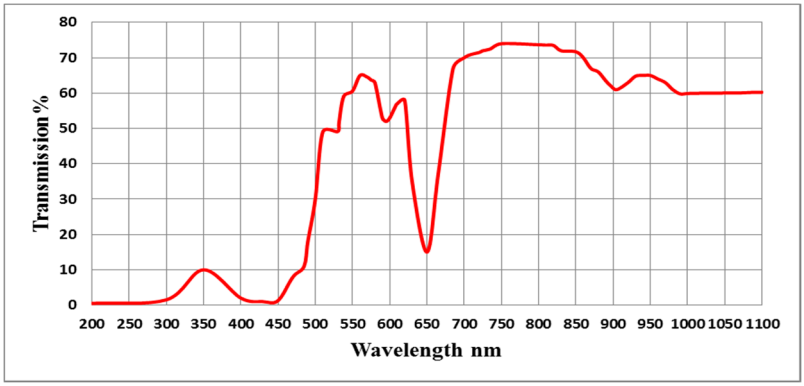

Figure 5. Olive oil transmission spectrum.

Preprints (www.preprints.org) | NOT PEER-REVIEWED | Posted: 17 November 2016 doi:10.20944/preprints201611.0088.v1

5. Fiber injection

The next step after the star line adhesive is chosen for making Bragg gating, a photonic crystal fiber (PCF) (HC19-1550) hollow core type has been used. This PCF consists of fiber core diameter 20μm, and there are air holes surrounding this fiber core, each hole has a diameter of 70 μm and cladding diameter of 115 μm. Bragg grating is made by injecting PCF with liquid mixture of adhesive material, olive oil and ethanol. Olive oil has higher viscosity as compared with the star line Glass Mechanix adhesive material and it must be diluted to mix with it. Therefore, ethanol is used with the liquid mixture because of the hydrophobic interactions between the hydro carbon chains in olive oil and ethanol causes the one with higher viscosity to dissolve. The olive oil is diluted with ethanol before being added to the photo adhesive material. Capillary action technique is being used for injecting the fiber in this research.

Four hollow core photonic crystal fibers were used.

- **PCF (A):** was injected with only star line Glass Mechanix adhesive material of volume (0.12 ml/cc).
- **PCF (B):** was injected with a volume (0.12 ml/cc) of liquid mixture consists from (0.06 ml/cc) star line Glass Mechanix adhesive material, (0.03 ml/cc) olive oil and (0.03 ml/cc) ethanol.
- **PCF (C)**: was injected with a volume (0.12 ml/cc) of liquid mixture consists from (0.04 ml/cc) star line Glass Mechanix adhesive material, (0.04 ml/cc) olive oil and (0.04 ml/cc) ethanol.
- **PCF (D):** was injected with a volume (0.12 ml/cc) of liquid mixture consists from (0.03 ml/cc) star line Glass Mechanix adhesive material, (0.06 ml/cc) olive oil and (0.03 ml/cc) ethanol.

6. Experimental Set up of the fabrication process

The experimental setup of the fabrication process is classified mainly into: the linear translation stage, the control unit and the optical system; It will be explained later in details. The experimental fabrication setup is shown in Figure 6.

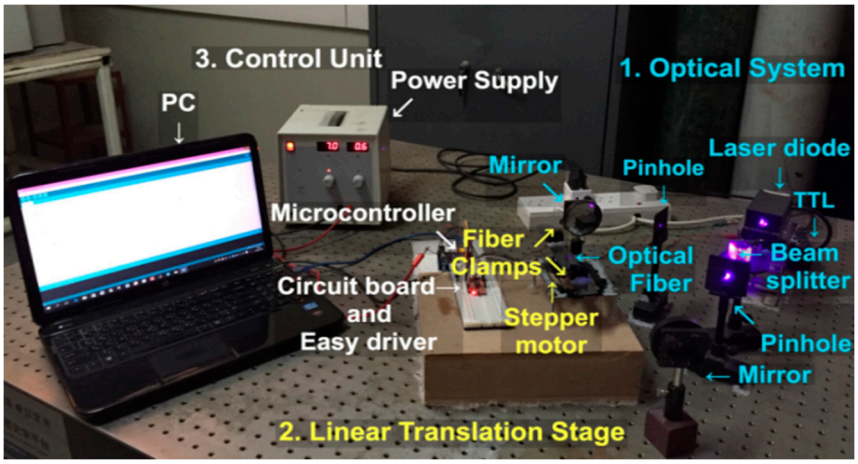

Figure 6. Experimental Fabrication set up.

The optical system consists of an optical source, two pinholes, two mirrors and beam splitter, as given in Figure 7. Each component has an exceptional importance for FBG fabrication.

Preprints (www.preprints.org) | NOT PEER-REVIEWED | Posted: 17 November 2016 doi:10.20944/preprints201611.0088.v1

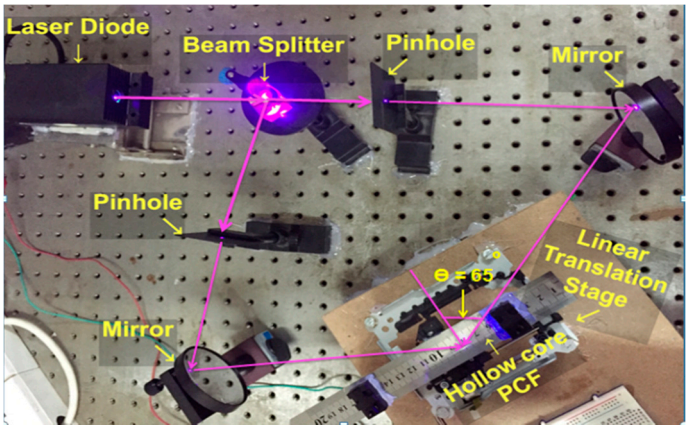

Figure 7. The path of the laser beam in the optical setup.

Optical source used for fabrication fiber Bragg grating is a continuous wave diode laser type (SDL-405-100T) functioned at 405 nm wavelength and 100 mW output power. It has a control unit used to switch it ON/OFF. The purpose of choosing this wavelength depends on the photosensitivity of the injected material inside the hollow core photonic crystal optical, i.e. this laser wavelength matched the spectrum of absorption of the star line adhesive that was injected in the PCF. The profile beam of the laser diode source used has elliptical shape. So, focusing this laser beam required reshaping the laser beam into circular shape. If the laser source is switched on, the path of the laser beam is followed through the optical elements as shown in Figure 7. The laser beam is directed to a beam splitter, where it is splitted into two laser beams of the same power. The beam splitter that is used has an incident angle about 45° in order to split the laser beam. After that these beams are directed to a dielectric mirrors to be reflected. These dielectric mirrors control the paths of the beams by adjusting these mirrors in x and in y axes. Then, these beams are recombined and creating interference fringes pattern inside the PCF core.

The linear translation stage is a stage moves linearly in z-axis only and it's consists of two fiber clamps and bipolar stepper motor as given in Figure 8.

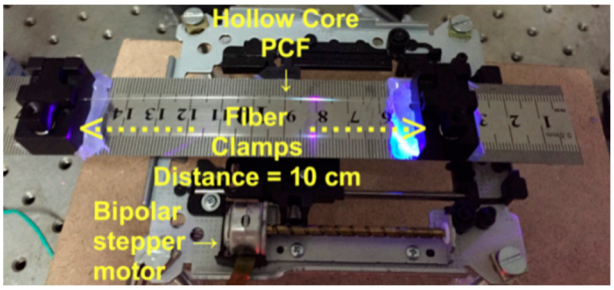

Figure 8. A translation stage that is moves linearly in z-axis.

The fiber is put on the stage and held by the fiber clamps. The distance separation between these clamps is 10 cm. The motor used in this stage is a bipolar Micro stepper motor, its two phase four wire hybrid type, this motor requires dc voltage supplier about 4-6 volt. The motor has a 15 mm diameter with SM15DD screw type and 9 mm height. The rod diameter and length are 3 mm and 52.5 mm respectively. The total distance of the movable stage is 3.8 cm in one direction and the motor is moved 158 full steps to complete this distance. Motor resolution is 240 μm for each step of the stepper motor.

Preprints (www.preprints.org) | NOT PEER-REVIEWED | Posted: 17 November 2016 doi:10.20944/preprints201611.0088.v1

The Control Unit consists of motor driver board (A3967 easy driver), microcontroller board (Arduino Uno R3), power supply to supply voltage to the motor driver board and personal computer.

The Arduino is programmed by the personal computer to switch the laser diode ON and OFF by TTL function of the laser drive and to control a bipolar stepper motor by sending signal to the bipolar stepper motor through A3967 easy driver. These signals control the stepper motor speed, steps, and direction. After sending these signals to the A3967 easy driver input signal port, then these signals pass from A3967 easy driver to the input ports bipolar stepper motor (A1, A2, B1, B2). Arduino Uno R3 is programmed to do the following sequence:

1. The laser is switched on by TTL function to script on the fiber for 3 minutes. To ensure that no movement or vibration occurs in place, the fiber is held firmly during this time.
2. The laser is switched OFF to stop the inscription process.
3. The fiber is moved by step resolution 240 μm. Then, the laser is switched ON again.

This procedure is repeated again until it covers the distance of 3.8 cm. The laser is still off for two second after each step to make sure that no additional inscription on the fiber happens through the steps movement. The total time of the inscription process of four fibers is about 32:30 hours.

7. Testing FBG setup for output detection and data recording

It is essential to detect and record the output data of Bragg reflected response from the PCFs to makes sure if the inscription of the FBG is completed correctly and also to obtain the value of reflected Bragg wavelength.

The 651.3 nm laser source is used for testing the functionality of the PCF. The fiber clamps are used to hold the PCF. The end of the PCF is placed in front of the laser source and the other end in front of an optical signal analyser (OSA) (Thorlabs-CCS200) for data analysis and recording. The OSA is a wavelength scanning device that can record the output detected power for each wavelength. It has internal charge coupled device (CCD) line array with 3648 pixel. It is also auto compensated for dark current noise and amplitude corrected. This OSA is sensitive to wavelengths ranges from 200 nm to 1000 nm. Different parameters can be varied for optimizing the output detected power. The OSA is used for detecting the output power of the desired wavelength before and after fabrication. The sensitivity of this OSA gives accurate data for sensing the effect of the FBG. When the light from the laser source entered the PCF, The fabricated Bragg grating in the PCF will reflect the wanted Bragg wavelength, so the OSA from the other end of the PCF will show the exact amount of power that is transmitted from these Bragg grating therefore Bragg reflected wavelength can be obtained from the transmission spectrum. The reflected wavelength couldn't be seen because it must have an optical circulator.

8. Results and Discussion (Part 1)

8.1 Microscopic images of the inscription PCFs

The next step after the process of inscription is to check PCFs visually, typically through an optical microscope. The images of the microscope shows different essential information about the PCFs properties for example the optical examination shows if the process of inscription is completed successfully. Furthermore, it displays the defects that might occur during the process of inscription. The inscription results on the four PCFs are illustrated in Figures (9-12).The Bragg grating appears in the cores of the four PCFs. Figure 9 shows PCF (A) with a 40X microscope image of fabricated FBG. It shows that PCF (A) didn't experience any break through the process of

Preprints (www.preprints.org) | NOT PEER-REVIEWED | Posted: 17 November 2016 doi:10.20944/preprints201611.0088.v1

inscription. If any break happened, it could be presented in the section of the fiber core. The image that is magnified displays a nearer view of PCF core. It shows the regions that are exposed to UV light successfully. These regions illustrate the fabricated Bragg grating inside the fiber core which is resulted from the interference of the two UV laser beams.

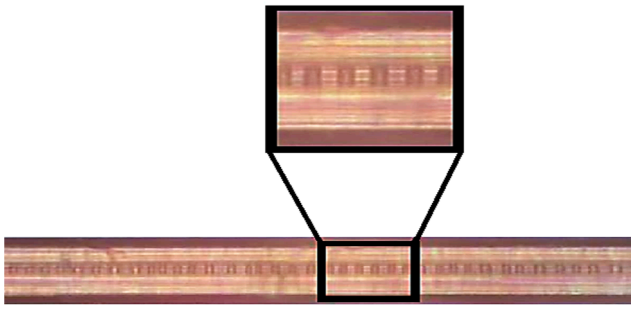

Figure 9. FBG of PCF (A) under optical microscope.

Figure 10 shows PCF (B) with a 40X microscope image of fabricated FBG. It shows that PCF (B) core didn't experience any break. It displays the regions that exposed to UV light gives less clear view than PCF (A) due to the density of olive oil.

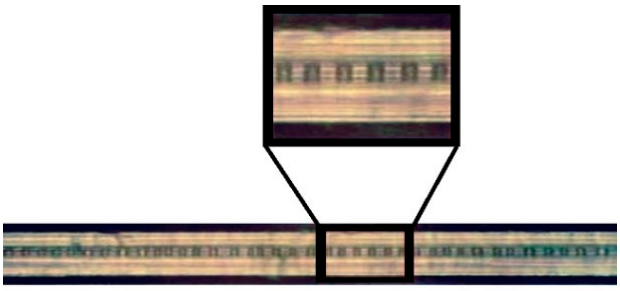

Figure 10. FBG of PCF (B) under optical microscope.

Figure 11 shows PCF (C) with a 40X microscope image of fabricated FBG. It show the regions that are cured by UV light are recognized hardly due to the higher density of olive oil than and PCF (B).

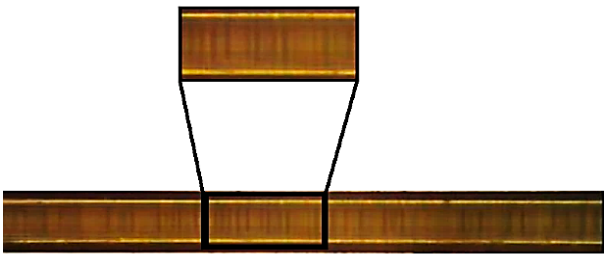

Figure 11. FBG of PCF (C) under optical microscope.

Figure 12 shows PCF (D) with a 40X microscope image of fabricated FBG. It shows the regions that are cured by UV light are most hardly recognized due to the higher density of olive oil than PCF (B) and PCF (C).

Preprints (www.preprints.org) | NOT PEER-REVIEWED | Posted: 17 November 2016 doi:10.20944/preprints201611.0088.v1

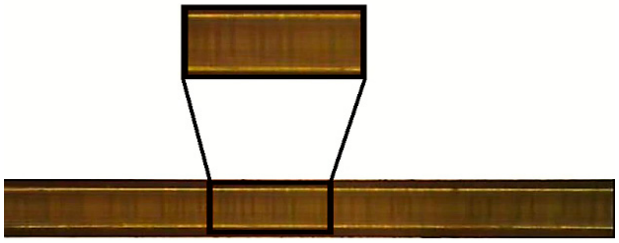

Figure 12. FBG of PCF (D) under optical microscope.

PCF (A) shows clearer grating period PCF (D) because the photosensitive material is higher in PCF (A).

8.2 The Optical Characterization

It is a process that gives the wavelength bands of the tested PCFs whether it works correctly. This is done by directing the laser light inside the PCFs. In this research, laser at wavelength 651.3 nm is used for the testing process. The output spectrum of a PCF without any grating inscription is shown in Figure 13 . It shows that, the laser directed through the PCF without any variation laser spectrum i.e. no reflection happens. This result is very important for comparison with inscrpited PCFs spectrums.

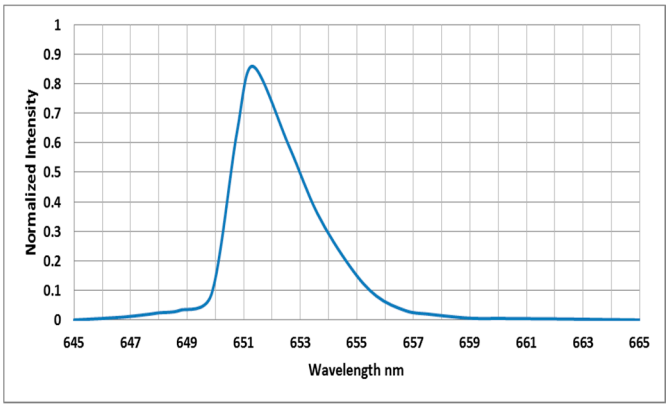

Figure 13. Spectrum of 651.3 nm diode laser after passing the hollow core PCF without any injected material.

The fabricated FBG using star line adhesive is verified by optical characterization. The output of the fabricated PCF (A) is presented in Figure 14. FBG length of all PCFs is 3.8 cm. As shown in Figure 14 the output laser peak shifts and reduce at 653.3551 nm, this wavelength shift from the setting wavelength 651.3 with half angle $\theta = 65°$ due to the setting error of the half angle (θ) between two interfering violet laser (405nm) correctly about 0.588% calculated from the following equation:

$$\% \text{ Error} = \left| \frac{\text{Theoretical } \theta - \text{Experimental } \theta}{\text{Theoretical } \theta} \right| \times 100$$

The experimental half angle is about $\theta = 64.62°$, the experimental half angle calculated using equation (12) by applying the values of the fabrication laser beam 405 nm, the effective refractive index of fiber (A), and the reflected Bragg wavelength of fiber (A). The effective refractive index of fiber (A) and the reflected Bragg wavelength are given in Table 1. This reduction of Bragg wavelength is because of the reflection from the periodic Bragg grating layers in the PCF core. As mentioned previously, the index of refraction and the grating period between layers determine the

Preprints (www.preprints.org) | NOT PEER-REVIEWED | Posted: 17 November 2016 doi:10.20944/preprints201611.0088.v1

Bragg reflected wavelength. So, by changing the period, the peak of Bragg reflected wavelength can be blue shifted or red shifted. However, the grating period is obtained using equation (12) using the interference created by the two violet laser beams 405 nm that is used in FBG fabrication and using the half angle (θ) between two interfering violet laser (405nm). The FBG quality is obtained via the sharpness or the width of the reflected Bragg wavelength. Figure 14 shows a sharp drop at wavelength 653.3551 nm expressing a high precision reflection and FWHM about 0.5 nm.

The second test of FBG fabrication of PCF (B) shows a higher reflection at 653.3555438 nm with more sharpness than the previous fabricated PCF (A) and with FWHM about 0.53 nm as shown in Figure 14. This shows that there is a stronger reflection from the periodic Bragg layers from the previous fabricated PCF (A). This strength resulted from the fact that liquid mixture is strongly cured when PCF core is irradiated by the violet laser.

The third test of FBG fabrication of PCF (C) shows a higher reflection at 653.3565367 nm with more sharpness than the previous two fabricated PCFs (A and B) with FWHM about 0.7 nm as shown in Figure 14. This shows that there is a strongest reflection from the periodic Bragg layers from the previous two fabricated PCFs. This strength comes from the fact that this mixture is much strongly cured when PCF core is irradiated by the violet laser.

The fourth test of FBG fabrication of PCF (D) shows the highest reflection at 653.3582 nm with much more sharpness than the previous fabricated PCFs (A, B, and C) with FWHM about 0.74 nm as shown in Figure 14. This shows that there is a much strongest reflection from the periodic Bragg layers from the previous fabricated PCFs. This strength comes from the fact that this mixture is much more strongly cured when PCF core is exposed to the laser irradiation.

The four fabricated PCFs spectrums comparisons show that, using the PCF (D) gives an enhanced output spectrum , generating a sharpest output with greater reflection depth and widest FWHM. Hence, decreasing Bragg grating length is necessary for the process of inscription because this will decrease the cost. i.e. to get the same results from PCFs (A, B, and D), Bragg grating length must be doubled or tripled and this effect on the cost and the time of the inscription process. The four PCFs output spectrums are presented in Figure 14.

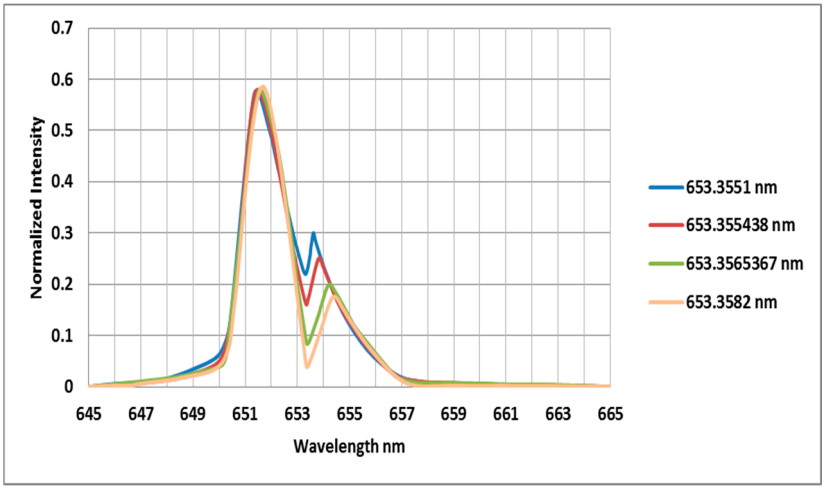

Figure 14. The spectrums of the four fabricated PCFs.

Preprints (www.preprints.org) | NOT PEER-REVIEWED | Posted: 17 November 2016 doi:10.20944/preprints201611.0088.v1

Table 1 gives the numerical examination of the four PCFs spectrums using the equations of the previous chapter. It's obvious that the Bragg reflected wavelength shift for the four PCFs are approximately similar with 0.001 nm difference. However, the variation of the indices of refraction is changes with little quantity for the four PCFs. The liquid mixtures FWHM is more than of the PCF (A).

Table 1. The variations between the four PCFs.

Injected material	λ_B (nm)	Δn^* 10^{-6}	n_{eff}	$\Delta\lambda$ (nm)	Reflectivity %	FWHM (nm)
PCF (A)	653.3551	7.623	1.45756812	2.0178723	76.20	0.5
PCF (B)	653.3555438	8.613	1.45756911	2.0183161	82.87532	0.53
PCF (C)	653.3565367	10.828	1.4575713250	2.019309	91.49684	0.7
PCF (D)	653.3582	14.985	1.457575482	2.0209723	96.09647	0.74

8.3 Reflected Bragg Wavelength simulation

Investigating FBG further, a simulation code is presented by the same parameters that used in the process of inscription. Simulation code (using MATLAB program) of Bragg reflected wavelength of PCF (A) is shown in Figure 15.

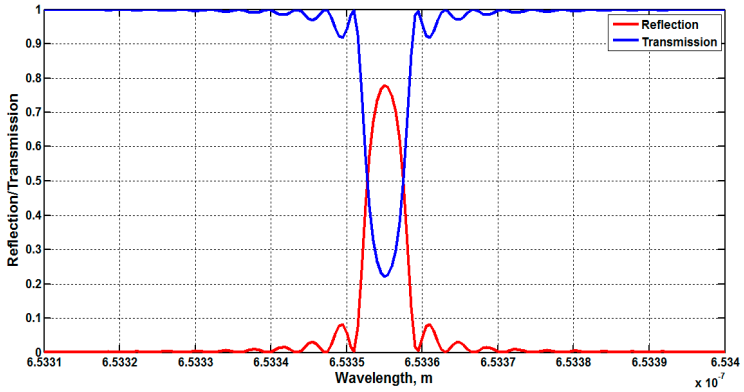

Figure 15. Reflection/Transmission of PCF (A).

The figure displays the reflection/transmission spectrum of the FBG by the coupled mode theory and the transfer matrix method (TMM) using equation (7). It also displays that the center wavelength of the reflection/transmission is at 653.3551 nm. The effective index of refraction used in this code is very similar to that in Table 1 which is obtained using experimental measurements. It also shows that, the reflectivity and transmissivity is about 77.81% and 22.19% respectively. If the grating length is increased about 9.8 cm then the reflectivity of PCF (A) will reach 100% as shown in Figure 16.

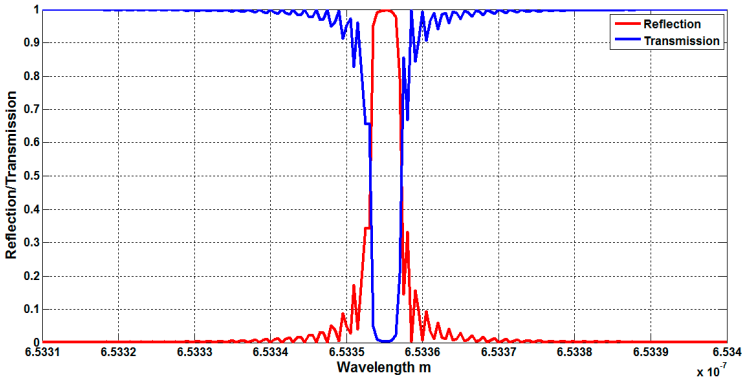

Figure 16. Reflection/Transmission of PCF (A) with grating length about 9.8 cm.

Preprints (www.preprints.org) | NOT PEER-REVIEWED | Posted: 17 November 2016 doi:10.20944/preprints201611.0088.v1

Figure 17 shows the simulation using the parameters of PCF (B).Simulation results show that Bragg reflected wavelength of the reflection/transmission is at 653.3555438 nm. The effective refractive index used in the code of simulation is very similar to that given in Table 1 which are obtained using experimental determinations. It also show that, the reflectivity and transmissivity is about 83.97% and 16.03% respectively for exact number of layers.

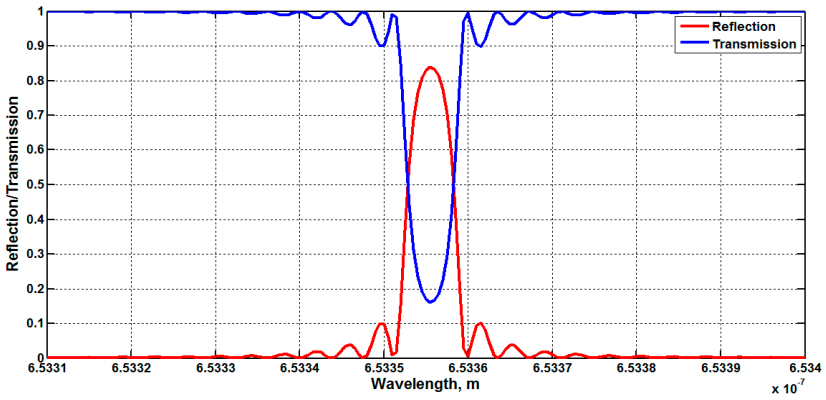

Figure 17. Reflection/Transmission of PCF (B).

Figure 18 shows the code of the simulation using the parameters of the PCF (C). Simulation results show that Bragg reflected wavelength of the reflection/transmission is at 653.3565367 nm. The effective refractive index used in the simulation code is very similar to that given in Table 1 which is obtained by experimental determinations. It also shows that, the reflectivity and transmissivity is about 92.5% and 7.5% respectively for exact number of layers.

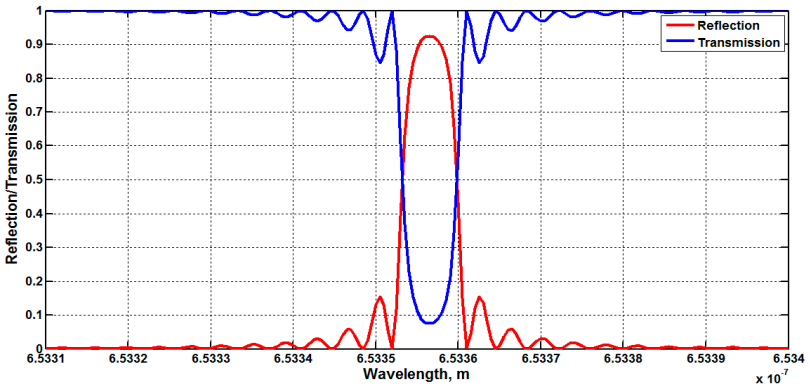

Figure 18. Reflection/Transmission of PCF (C).

Figure 19 shows the simulation using the parameters of PCF (D). Simulation results show that Bragg reflected wavelength of the reflection/transmission is at 653.35582 nm. The effective refractive index that is used in the simulation code is very similar to that given in Table 1 which is obtained by by experimental determinations. It also shows that, the reflectivity and transmissivity is about 98.28% and 1.72% respectively for exact number of layers.

Preprints (www.preprints.org) | NOT PEER-REVIEWED | Posted: 17 November 2016 doi:10.20944/preprints201611.0088.v1

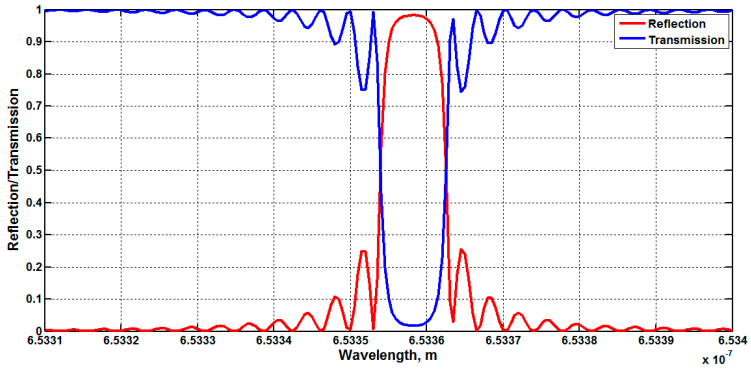

Figure 19. Reflection/Transmission of PCF (D).

It can be noticed from the previous simulations that PCF (D) has the highest reflection due the volume of olive oil because it has the absorbance peak appear at the reflected Bragg wavelength and emission peak when the material excited at same wavelength as shown in Figure 20 [7].

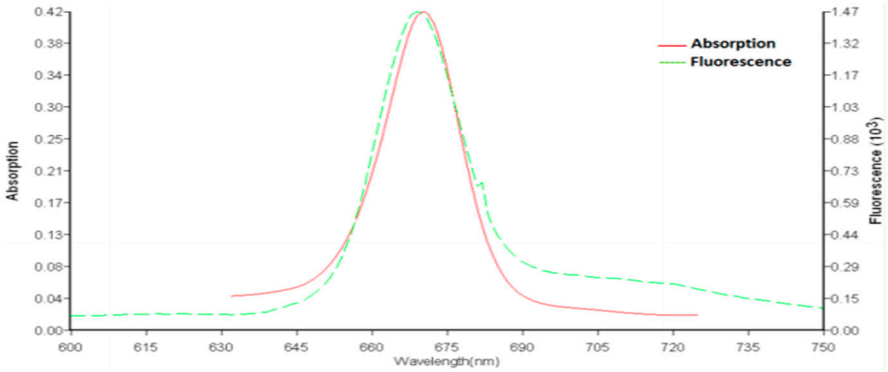

Figure 20. The absorbance peak of olive oil appears at wavelength 669nm and its emission peak when the material excited at that wavelength [7].

9. Experimental Setup of Magnetic Field Sensor :

The experimental setup and of the magnetic field sensor as shown in Figure 21 used to test the magnetic field sensing on fiber Bragg grating by measuring Bragg reflection wavelength shift of three types of PCFs (B, C and D).

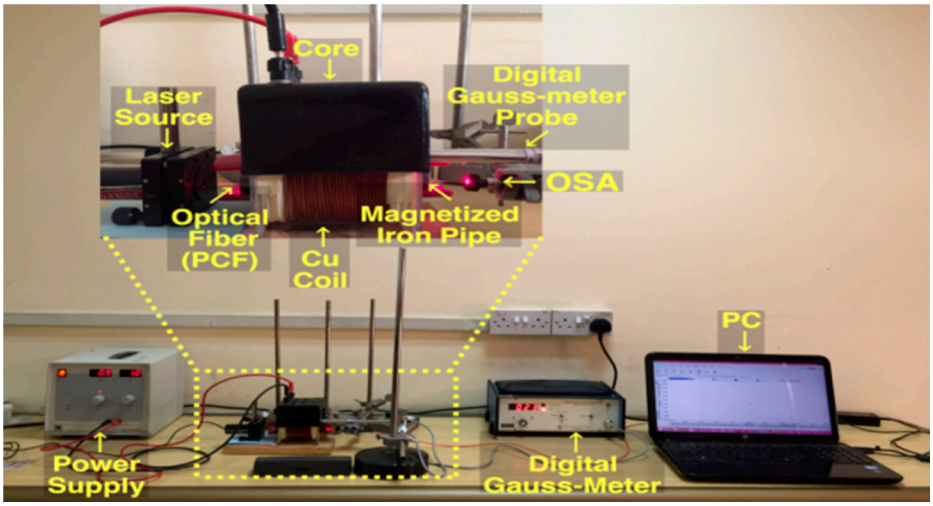

Figure 21. The experimental set up of magnetic field sensor.

Preprints (www.preprints.org) | NOT PEER-REVIEWED | Posted: 17 November 2016 doi:10.20944/preprints201611.0088.v1

The experimental set up shown in Figure 21 consists of:

1. Laser diode source of 650 nm wavelength is used to generate the light inside an optical fiber.
2. Power supply is used to generate the magnetic field by changing the electrical current values from 1A to 5 A at a certain voltages.
3. Core with a copper coil is connected to the power supply in order to generate the magnetic field inside an iron pipe of 10 cm length.
4. Photonic crystal fiber held inside the magnetized iron pipe is used to test magnetic sensitivity i.e. measuring Bragg reflection wavelength shift in the presence of the magnetic field.
5. Digital Gauss-meter (DGM-202) with an axial probe is used to measure the magnetic flux density.
6. Optical spectrum analyzer (OSA) (Thorlabs-CCS200) is used for data analysis and recording.
7. PC is used to display the data analysis and recording.

First, the power supply was set at voltage value where the current reaches 1A, then the magnetic flux density value is measured with the digital Guass-meter axial probe, after that Bragg reflection wavelength shift is measured with the OSA from the output light of the laser source after it passing through an optical fiber, and then the current is set at values of 2, 3, 4, and 5 A. The previous procedure of measuring the magnetic flux density and Bragg reflection wavelength shift for each current value are repeated for PCF (B). The two others PCFs (C) and (D) followed the same procedure of the first PCF (B).

10. Results and Discussion (Part 2)

10.1. The Optical Characterisation results of testing the magnetic field sensor of the three PCFs:

The experimental set up of magnetic field sensor in Figure 21 was used to measure the optical characterizations of Bragg reflection wavelengths shifts spectrums of the three PCFs. These spectrums are obtained by changing the magnetic flux (0 Gauss - 93 Gauss), where the magnetic flux density and Bragg reflection wavelength shift was calculated for each current value using axial probe and OSA respectively.

10.1.1. PCF (B) Bragg Reflected Wavelength Shifts

Figure 22 shows the difference between the spectrums of Bragg reflected wavelength shifts of PCF (B). Table 2 gives more information about the numerical examination of these spectrums.

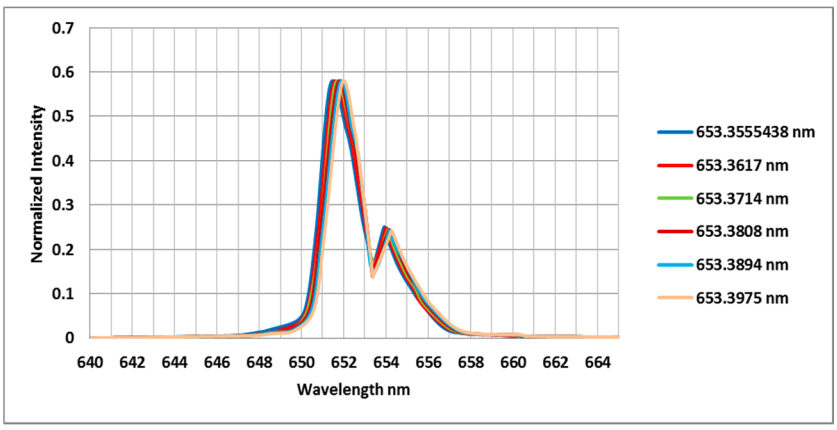

Figure 22. The spectrums of Bragg reflected wavelength shifts of PCF (B).

Preprints (www.preprints.org) | NOT PEER-REVIEWED | Posted: 17 November 2016 doi:10.20944/preprints201611.0088.v1

Table 2. The numerical examination of PCF (B).

Magnetic Flux density (Gauss)	λ_B (nm)	Reflectivity %	FWHM (nm)
0	653.3555438	82.87532	0.53
21	653.3617	82.95165	0.5302
39	653.3714	83.07888	0.5305
60	653.3808	83.20611	0.5308
76	653.3894	83.50120	0.5312
92	653.3975	83.62341	0.5315

10.1.2. PCF (C) Bragg Reflected Wavelength Shifts

Figure 23 shows the difference between the spectrums of Bragg reflected wavelength shifts of PCF (C). Table 3 gives more information about the numerical examination of these spectrums.

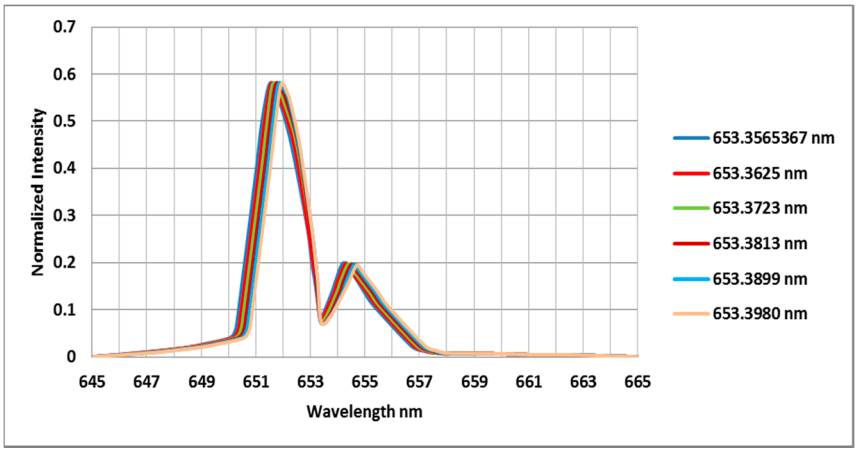

Figure 23. The spectrums of Bragg reflected wavelength shifts of PCF (C).

Table 3. The numerical examination of PCF (C).

Magnetic Flux density (Gauss)	λ_B (nm)	Reflectivity %	FWHM (nm)
0	653.3565367	91.49684	0.7
22	653.3625	92.13524	0.8
42	653.3723	92.4878	0.85
58.5	653.3813	92.54204	0.88
77	653.3899	92.58724	0.92
93	653.3980	92.67764	0.97

Preprints (www.preprints.org) | NOT PEER-REVIEWED | Posted: 17 November 2016 doi:10.20944/preprints201611.0088.v1

10.1.3. PCF (D) Bragg Reflected Wavelength Shifts

Figure 24 shows the difference between the spectrums of Bragg reflected wavelength shifts of PCF (D). Table 4 gives more information about the numerical examination of these spectrums.

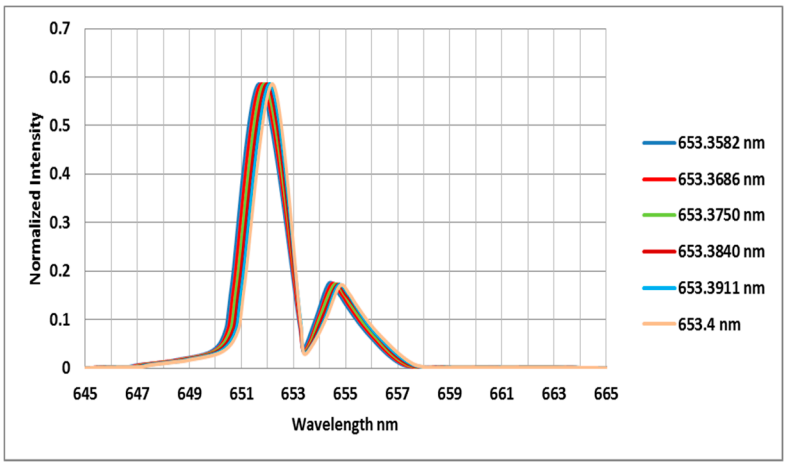

Figure 24. The spectrums of Bragg reflected wavelength shifts of PCF (D).

Table 4. The numerical examination of PCF (D).

Magnetic Flux density (Gauss)	λ_B (nm)	Reflectivity %	FWHM (nm)
0	653.3582	96.09647	0.74
22	653.3686	96.50737	0.83
41	653.3750	96.61009	0.86
60	653.3840	96.71282	0.89
78	653.3911	96.81554	0.94
93	653.4	96.91827	0.98

The curves between magnetic flux density and Bragg reflection wavelengths shifts of three PCFs with different volumes of liquid mixture were determined as shown in Figure 25.

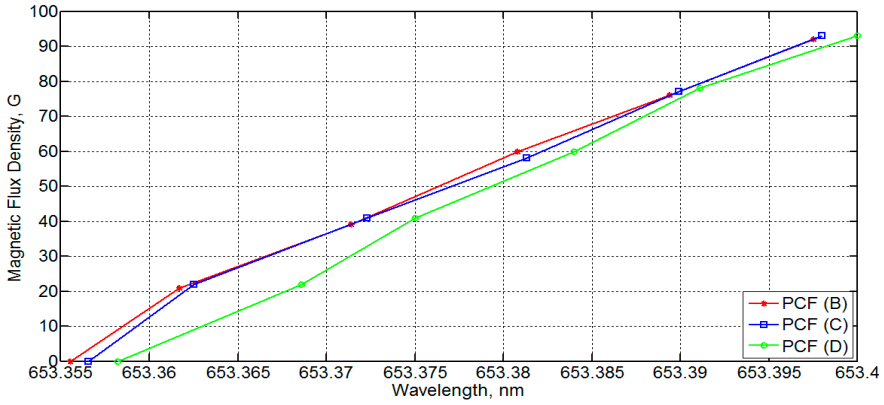

Figure 25. Comparison curve between the magnetic flux density versus Bragg reflection wavelength shift of three PCFs (B, C, and D).

The curves in Figure 25 show that increasing the magnetic flux density is due to the linear relation with the electrical current leads to Bragg reflection wavelengths shifts of the three PCFs to NIR range as mentioned previously and not to UV range this is happened because olive oil has a positive Verdet constant equals to (98.6808 rad/T. m) at the Bragg reflected wavelength [8].

As seen in Figure 25 the PCF (D) has the greatest wavelength shift sensitivity about (0.000494623656 nm/ Gauss) than the two others PCFs (B and C) about (0.0004560456522 nm/Gauss) and (0.000482518919 nm/Gauss) respectively, this is happened due to olive oil different volumes in the three PCFs, because olive oil is a photonic crystal material, therefore a PCF with larger volume of olive oil has the greatest wavelength sensitivity.

11. Conclusions

The important facts concluded from the practical results of this work can be given as follow:

1. The fabrication setup is able to fabricate Bragg grating in four PCFs filled with liquids of different volumes consisting of olive oil, star line Glass Mechanix adhesive material and ethanol using amplitude interferometric technique with Bragg reflection wavelength of (λ_B) 653.3 nm and reflectivity ranges equal to (PCF(A) =76.20 %, PCF (B) =82.87532 %, PCF (C) =91.49684 %, PCF (D) = 96.09647 %). It is designed and implemented successfully.
2. The half angle of the two interfering UV beams (θ) in amplitude interferometric technique and the grating period (Λ) controls the designed Bragg reflected wavelength (λ_B).
3. Increasing the volume of olive oil in the liquid mixture that injected inside PCFs gives a greater shift in the fabricated Bragg reflected wavelength due to the nonlinearity of olive oil.
4. The simulation results show increasing in the volume of olive oil for the liquid mixture that injected inside PCFs giving the highest reflectivity because olive oil has an absorbance peak and an emission peak when the material excited at this fabricated Bragg reflected wavelength [7].
5. The application of magnetic field sensor results show that increasing the magnetic flux density will increase the shift of Bragg reflected wavelength. As well as increasing olive oil volume in the liquid mixture that injected inside PCFs giving the greatest wavelength shift to NIR range because olive oil at this fabricated Bragg wavelength has positive Verdet constant equals to (98.6808 rad/T. m) [8], so this fiber is more sensitive compared to other fibers.
6. Increasing olive oil volume for the liquid mixture that injected inside PCFs giving the greatest wavelength shift sensitivity about (0.000494623656 nm/ Gauss). The FWHM is increased by the increasing of wavelength shift for all PCFs. The shift of wavelength due to the magnetic field is a linear shift. The reflectivity increases when the magnetic flux density increases.

References

1. Othonos, A. Fiber Bragg gratings. *Review of Scientific Instruments: American Institute of Physics* 1997, *Vol. 68*, pp. 4309-4341. Available Online: http://dx.doi.org/10.1063/1.1148392 (12 September 1997).
2. Othonos, A.; Kalli, K. *Fiber Bragg Gratings: Fundamentals and Applications in Telecommunications and Sensing*, Artech House, Norwood, MA, 1999, ISBN 0-89006-344-3.
3. Allil, R. C. S. B.; Werneck, M. M.; Ribeiro, B. A.; de Nazaré, F. V. B.; A Guide to Fiber Bragg Grating Sensors In *Current Trends in Short- and Long-period Fiber Gratings*, Laborde, C. C., Eds.; InTech, 2013, DOI: 10.5772/54682.

Available Online: http://www.intechopen.com/books/current-trends-in-short-and-long-period-fiber-gratings/a-guide-to-fiber-bragg-grating-sensors (15 May 2013).

4. Lam, D. K. W.; Garside, B. K. Characterization of single-mode Optical fiber filters. *Appl. Opt.* 1981, *Vol. 20*, pp. 440-445.
5. Marcuse, D. Loss Analysis of Single-Mode Fiber Splices. *The Bell System Technical Journal* 1977, *Vol. 56*, Pages: 703-718.
6. Meltz, G.; Morey, W.W.; Glenn, W. H. Formation of Bragg gratings in optical fibers by a transverse holographic method. *Optics Letters* 1989, *Vol. 14*, pp. 823-825.
7. Mohammed, O. N.; AL – Dergazly A. A. Measurement the Fluorescence Parameters of the Olive Oil and comparing it with Some Laser Dye Materials. *Journal of Engineering* 2010, *Vol. 16*, Pages: 4527-4534.
8. Shakir, A.; AL-Mudhafa, R.D.; Al-Dergazly A. Verdet Constant Measurement of Olive Oil for Magnetic Field Sensor. *International Journal of Advances in Electrical & Electronics Engineering* 2013, *Vol. 2*, Pages: 362-368.